Available online at www.sciencedirect.com
ScienceDirect
Journal of Sound and Vibration 300 (2007) 330–344
JOURNAL OF SOUND AND VIBRATION
www.elsevier.com/locate/jsvi

Determining the effect of detuning parameters on the absorption region for a coupled nonlinear system of varying orientation

Mustafa Yaman*, Sadri Sen

Department of Mechanical Engineering, Ataturk University, Erzurum, Turkey

Received 20 April 2006; received in revised form 15 August 2006; accepted 17 August 2006
Available online 10 October 2006

Abstract

In this study, the nonlinear behavior of a slender beam coupled with a pendulum is investigated numerically in terms of different system parameters. The structure consisting of a cantilever beam of varying orientation with a tip mass and pendulum which is attached to the tip mass as a passive vibration absorber is subjected to a vertical sinusoidal base excitation. The Euler–Bernoulli theory for the slender beam is used to derive the governing non-linear partial differential equation. The non-linear terms arising from inertia, curvature and axial displacement caused by large transverse deflections, and the coupling between the primary structure and absorber are retained up to third order. When the structure is forced in the neighborhood of its resonance, the pendulum absorber (controller) reduces the structure response because of autoparametric interaction between the beam and pendulum. Autoparametric interaction in the system was investigated by varying orientation angles, the forcing amplitude, the internal frequency ratio, and the mass ratio in the neighborhood of the autoparametric resonance. The absorption regions were defined with respect to the system parameters for the passive vibration absorber.

1. Introduction

In the past, vibration of flexible beams and columns, with appendages attached along the span had been studied by a number of authors. Zavodney and Nayfeh [1] investigated the dynamics of a cantilever beam carrying a lumped mass. They modeled the structure with cubic geometric and inertia nonlinearities. Crespo da Silva et al. [2] studied the problem of determining the equilibrium of a beam with a tip mass and the frequency of infinitesimally small oscillations about the equilibrium state of the beam. They reported that the natural frequency can be unsatisfactory for large values of the tip mass. Haxton and Barr [3] studied a flexible column with tip mass fixed to a heavy block undergoing parametric vibration. As a result, the nonlinear coupling between the spring-mass system and the tip-weighted beam acted as an energy bridge that transferred energy from the periodic forcing of the spring-mass system into beam deflections. Ertas et al. [4] investigated experimentally an orientable flexible beam with a tip mass and pendulum. They determined an orientation

*Corresponding author. Tel.: +90 442 231 4862; fax: +90 442 236 0957.
E-mail address: myaman@atauni.edu.tr (M. Yaman).

0022-460X/$ - see front matter © 2006 Elsevier Ltd. All rights reserved.
doi:10.1016/j.jsv.2006.08.016

Nomenclature

c	damping coefficient of the beam
c_p	damping coefficient of the pendulum
E	modulus of elasticity
F_{pv}, F_{pu}	pendulum forces acting upon the beam at y and x-direction, respectively
F_{bv}, F_{bu}	beam forces acting upon the pendulum at y and x-direction, respectively
I	Moment of inertia
ℓ_p	length of the pendulum
L	length of the beam
m	total mass of the tip and pendulum
m_p	pendulum mass
m_T	tip mass
$q(t)$	time modulation of the beam
Q_v, Q_u	generalized forces acting upon the beam at y and x-direction
R_{ext}, R_{eff}	external and effective forces
s	arc-length along the beam
$u(s, t)$	relative displacement of the beam at x-direction
$v(s, t)$, $w(s, t)$	relative displacement of the beam at y-direction
x, y	fixed co-ordinate axis
X, Y	fixed global co-ordinate axis
$\ddot{y}_g(t)$	base acceleration
$\ddot{y}_{gv}$, $\ddot{y}_{gu}$	base acceleration at y and x directions, respectively
α	orientation angle of the beam
$\theta(s, t)$	angle of the deflection of the beam with x-axis
ρA	mass of the beam per unit length
ω_b	circular frequency of the beam
ω_p	circular frequency of the pendulum
Ω	forcing frequency
$\psi(t)$	pendulum angular displacement

boundary up to which the pendulum is effective, and showed that this boundary depends on forcing amplitude.

A useful technique for the elimination of undesirable vibration of problems of structural dynamics and machinery dynamics has been the application of one or more passive dynamic vibration absorbers. Currently, the most widely used passive vibration absorbers in engineering include: tuned mass absorbers, impact absorbers, pendulum-type absorbers, beam absorbers, and last but not least, liquid absorbers. The previous activities in the area of design, development, and application of tuned vibration absorbers were provided by Sun et al. [5]. Jacquot [6] developed a technique that gives the optimal dynamic vibration absorber parameters for the elimination of the excessive vibration in sinusoidal forced Bernoulli–Euler beams. Kitis et al. [7] proposed an efficient optimal design algorithm for minimizing the vibratory response of a multi-dof system under sinusoidal excitation over several excitation frequencies. Jordanov and Cheshnakov [8] used an algorithm to obtain optimal parameters for both linearly and nonlinearly damped dynamic vibration absorbers. Dahlberg [9] investigated three types of vibration absorbers: classical single-degree-of-freedom (sdof) absorbers, two sdof discrete absorbers, and a continuous cantilever beam absorber. The author clearly shows that the continuous vibration absorber is more effective than the other two absorbers.

In the literature, autoparametric vibration absorbers have been studied extensively for structural and machinery systems under sinusoidal and random excitation. Cuvalci [10] studied the dynamic behavior of a beam–pendulum system subjected to a periodic excitation. They investigated an absorption region numerically and experimentally with respect to forcing amplitude, internal frequency ratio and mass ratio for the passive vibration absorber. Yaman and Sen [11] studied the orientation effect of nonlinear flexible systems on performance of the pendulum absorber. They determined the effectiveness of pendulum-type passive vibration absorber attached to a primary structure whose orientation varies. The orientation at which the absorber is effective was established, and the factors that affect performance of the absorber were determined. Bishop et al. [12] investigated the parametrically driven pendulum in a large variety of stable periodic and chaotic motions for hanging and inverted equilibrium states. The existence of the periodic and chaotic attractors was verified numerically and experimentally. Queini et al. [13] investigated an active nonlinear vibration absorber for flexible structures (cantilever beam). The authors assumed an mdof system with quadratic nonlinearities that possesses two-to-one autoparametric resonances. They developed the equation of motion with quadratic

nonlinearities and analyzed the system through perturbation techniques and a numerical simulation. The authors also carried out several experiments and compared the results.

In this paper, the nonlinear system of varying orientation consisting of a flexible beam with an appendage that has a mass—passive vibration absorber (controller) attached to its tip has been investigated numerically. This type of device may find widespread application in, for instance, robot arm, antenna, and large space stations, where heavy sensitive equipment may have to be moved by long flexible arms. Any small motion of the base results in large amplitude vibrations, causing damage to the equipment. Therefore, to absorb vibrations of the system, a simple pendulum that is capable of absorbing large portion energy is attached to the main system. The main objective of this study is to investigate the effects over the absorption region of the orientation angle, the forcing amplitude, the internal frequency ratio, and the mass ratio. The nonlinear equations of motion were development to investigate the autoparametric interaction between the beam and pendulum. A series of parametric numerical studies were performed to study the response of the system under sinusoidal excitation. To investigate the nonlinear dynamics under autoparametric conditions ($\Omega = \omega_b = 2\omega_p$), the internal frequency ratio was varied between 0.46 and 0.54, the mass ratio varied between 0.1 and 1.0, and the forcing amplitude varied between 0.0001 and 0.001 for different orientation angles.

2. Equations of motion of the beam and pendulum

In this section, we derived the governing equation of motion using the Euler–Bernoulli theory. We assumed that the thickness of the beam/column is so small compared with the length that the effects of shearing deformation and rotatory inertia of the beam/column can be neglected [9]. The differential equations governing the flexural motion of inextensional beams, taking into account all the geometric nonlinearities in the system, were formulated in Zavodney and Nayfeh [1], and in Cuvalci [10]. A brief derivation of the equations for an inextensional beam-tip mass with a pendulum is presented below. The beam is assumed to be initially straight, of length L, and of constant mass ρA per unit length and constant stiffness. The quantity EI, where E is Young's modulus of the material and I is the principal cross-sectional area moments of inertia, is the bending stiffness of the beam and α is the orientation angle of the beam. The deformed beam is shown in Fig. 1. Let $u(s,t)$ and $v(s,t)$ denote the components along the inertial directions (x,y) of the displacement of the beam's centroidal axis C (which is assumed to be coincident with the beam's elastic axis) of a cross-section A due to elastic deformation of the beam. s is used to denote arc-length along the beam, t is the dimensional time, $y_g(t)$ is the base displacement. For inextensional beams, $(1+u')^2+v'^2 = 1$ where $(\,)' = \partial(\,)/\partial s$. The total axial displacement is

$$u(s,t) = \int_0^s (\sqrt{1-v'^2} - 1)\,\mathrm{d}s + y_{\mathrm{gu}}. \tag{1}$$

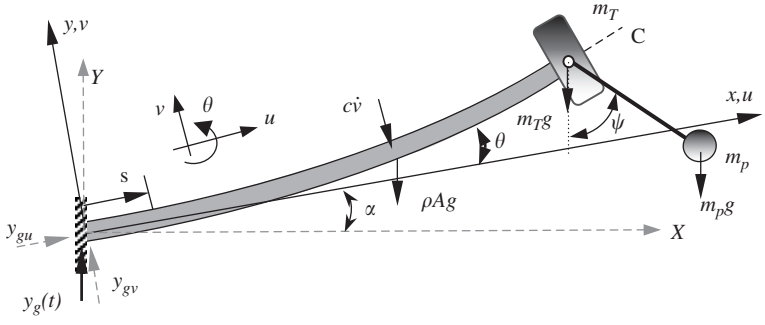

Fig. 1. Cantilever beam–pendulum with a concentrated mass subjected to vertical base motion.

The governing equations of motion and boundary conditions can be obtained from Hamilton's extended principle as in Crespo da Silva et al. [2], i.e.

$$\delta I = \int_{t_1}^{t_2} (\delta L_1 + \delta W_1)\,\mathrm{d}t + \int_{t1}^{t2} \{m[\dot{u}\,\delta\dot{u} + (\dot{v} + \dot{y}_{\mathrm{gv}})\,\delta\dot{v}] + F_{\mathrm{pv}}\delta v - [F_{\mathrm{pu}} + mg\,\sin(\alpha)]\delta u\}_{s=L}\,\mathrm{d}t = 0, \tag{2}$$

$$L_1 = \frac{1}{2}\int_0^L \{\rho A[(\dot{v} + \dot{y}_{\mathrm{gv}})^2 + \dot{u}^2] - EI(v''^2 + v''^2 v'^2) + \lambda(1 - (1 + u')^2 - v'^2)\}\,\mathrm{d}s, \tag{3}$$

where λ is a Lagrange multiplier, F_{pv}, F_{pu} are the pendulum forces acting upon of the beam at y- and x-direction, respectively, m is the sum of the tip and pendulum mass

$$\delta W_1 = -\int_0^L (\rho A g\,\sin(\alpha)\delta u + c\dot{v}\,\delta v)\,\mathrm{d}s. \tag{4}$$

L_1 and δW_1 are the Lagrangean and the virtual work for motion, respectively and c is the damping coefficient of the beam. Dots in the equations denote the differentiation with respect to time, t. For simplicity, it is assumed that the beam is slender, and that its torsional frequencies are much higher than its flexural frequencies, so that the small effects of rotary inertia and torsional dynamics are neglected. By carrying out the variations in Eq. (2), the differential equations of motion and a boundary condition equation governing the motion of the beam are readily obtained. The differential equations of motion are:

$$\rho A(\ddot{v} + \ddot{y}_{\mathrm{gv}}) + EIv'''' + EI(v'(v'v'')')' - [\lambda v']' = Q_v = -c\dot{v}, \tag{5}$$

$$\rho A\ddot{u} - [\lambda(1 + u')]' = Q_u = -\rho A g\,\sin(\alpha). \tag{6}$$

The associated boundary conditions obtained from Eq. (2) can be written as

$$u(0,t) = 0, \quad v(0,t) = 0 \text{ and } v'(0,t) = 0 \quad \text{at the fixed end, } s = 0, \tag{7}$$

$$\lambda((1 + u'))_{s=L} = -F_{\mathrm{pu}} - mg\,\sin(\alpha) - m\ddot{u}_{s=L},$$

$$EIv''(L,t) = 0,$$

$$EIv'''(L,t) + mg\,\sin(\alpha)v'(L,t) = m(\ddot{v} + \ddot{y}_{\mathrm{gv}})_{s=L} - F_{\mathrm{pv}} \text{ at the free end, } s = L. \tag{8}$$

Eqs. (5), (6) and the constraint relation, $(1+u')^2+v'^2 = 1$, govern the flexural motion of the beam when the torsional frequencies are much higher than the bending frequencies.

By making use of the cantilever boundary conditions, Eq. (6) can be integrated once to yield

$$\lambda(s,t) = \frac{1}{1+u'}\left[-\int_s^L \rho A\ddot{u}\,\mathrm{d}s + \int_s^L Q_u\,\mathrm{d}s - F_{\mathrm{pu}} - mg\,\sin(\alpha) - m\ddot{u}_{s=L}\right]. \tag{9}$$

Substitution Eq. (9) into Eq. (5) yields the following integro-partial differential equation for $v(s, t)$:

$$\begin{aligned}\rho A(\ddot{v} + \ddot{y}_{\mathrm{gv}}) + EIv'''' + EI\left[v'(v'v'')'\right]' + \left[v'\left(\int_s^L \rho A\ddot{u}\,\mathrm{d}s\right)\right]' - \left[v'\left(\int_s^L Q_u\,\mathrm{d}s\right)\right]' \\ - [v'(-F_{\mathrm{pu}} - mg\,\sin(\alpha) - m\ddot{u}_{s=L})]' = -c\dot{v}.\end{aligned} \tag{10}$$

Differentiating Eq. (1) twice with respect to time, and substituting into Eq. (10) yields

$$\begin{aligned}\rho A\ddot{v} + c\dot{v} + EIv'''' + EI[v'(v'v'')']' - \frac{1}{2}\rho A\left[v'\int_s^L \frac{\partial^2}{\partial t^2}\int_0^s v'^2\,\mathrm{d}s\,\mathrm{d}s\right]' - \frac{1}{2}m\left[v'\frac{\partial^2}{\partial t^2}\int_0^L v'^2\,\mathrm{d}s\right]' \\ + [v'\rho A(L-s)]'\{\ddot{y}_{\mathrm{gu}} + g\,\sin(\alpha)\} + m[v']'\{\ddot{y}_{\mathrm{gu}} + g\,\sin(\alpha)\} + F_{\mathrm{pu}}[v']' + \rho A\ddot{y}_{\mathrm{gv}} = 0.\end{aligned} \tag{11}$$

In this equation, the terms in the first bracket are the static hardening nonlinearities which arise from the potential energy stored in bending (nonlinear curvature), those in the second and third bracket are the inertial nonlinearities, with a net softening effect, due to the kinetic energy of axial motion. Eq. (11) is in full

agreement with the planar version of the equation derived by Crespo da Silva et al. [2] using the extended Hamilton principle, if we ignore F_{pu}, F_{pv} and gravitational effects as well as $\alpha = 0$.

2.1. Time-dependent boundary conditions

In many cases the boundary conditions are not homogeneous but time dependent. In our case, it is not difficult to see that the boundary condition at $s = L$ is not homogeneous. We shall attempt to find a solution of the problem by transforming it into a problem consisting of homogeneous boundary conditions. To this end, let us assume a solution of the problem described by Eq. (11) in the form below [17]

$$v(s,t) = w(s,t) + \hbar(s)P(t) \tag{12}$$

so that, we transform the problem for the variable $v(s,t)$ into a problem for variable $w(s,t)$. The function $\hbar(s)$ is chosen to render the boundary conditions for the variable $w(s,t)$ homogeneous.

So the boundary conditions for $w(s,t)$ are:

$$w(0,t) = -\hbar(0)P(t) \text{ and } w'(0,t) = -\hbar'(0)P(t), \tag{13}$$

$$\begin{aligned}\{EIw'''(s,t) - m\ddot{w}(s,t)\}\big|_{s=L} + mg\,\sin(\alpha)w'(s,t)\big|_{s=L} &= P(t) - \{EI\,\hbar'''(s)P(t)\}\big|_{s=L} \\ - mg\,\sin(\alpha)\hbar'(s)P(t)\big|_{s=L} &+ \{m\hbar(s)\ddot{P}(t)\}\big|_{s=L},\end{aligned} \tag{14}$$

where $P(t)$ is $m\ddot{y}_{\mathrm{gv}}(t) - F_{\mathrm{pv}}$.

To render the boundary conditions homogeneous, we must have

$$\hbar(0) = 0,\ \hbar'(0) = 0,\ EI\,\hbar'''(s)\big|_{s=L} = 1,\ \hbar''(s)\big|_{s=L} = 0,\ \hbar'(s)\big|_{s=L} = 0,\ \hbar(s)\big|_{s=L} = 0. \tag{15}$$

Considering the conditions above, the third of the boundary conditions can be written as

$$\frac{\mathrm{d}^3\hbar(s)}{\mathrm{d}s^3} = \frac{1}{EI}H[s-(L-\varepsilon)], \tag{16}$$

where $H[s-(L-\varepsilon)]$ is a Heaviside function and ε is a small quantity. The solution of the $\hbar(s)$ is given as

$$\hbar(s) = \frac{1}{6EI}[s-(L-\varepsilon)]^3 H[s-(L-\varepsilon)]. \tag{17}$$

The transformed problem consists of the nonhomegenous differential equation and homogeneous boundary conditions:

$$\begin{aligned}&\rho A\ddot{w} + c\dot{w} + EI\left\{w'''' + \left[\frac{1}{6EI}[s-(L-\varepsilon)]^3 H[s-(L-\varepsilon)]\right]'''' P(t)\right\} + EI(w'(w'w'')')' \\ &- \frac{1}{2}\rho A\left[w'\int_s^L \frac{\partial^2}{\partial t^2}\int_0^s w'^2\,\mathrm{d}s\,\mathrm{d}s\right]' - \frac{1}{2}m\left[w'\frac{\partial^2}{\partial t^2}\int_0^L w'^2\,\mathrm{d}s\right]' + [w'\rho A(L-s)]'(\ddot{y}_{\mathrm{gu}} + g\,\sin(\alpha)) \\ &+ m[w']'(\ddot{y}_{\mathrm{gu}} + g\,\sin(\alpha)) + F_{pu}[w']' + \rho A\ddot{y}_{\mathrm{gv}} = 0,\end{aligned} \tag{18}$$

where

$$\left[\tfrac{1}{6}[s-(L-\varepsilon)]^3 H[s-(L-\varepsilon)]\right]'''' = \delta[s-(L-\varepsilon)]. \tag{19}$$

The equation of the pendulum, obtained by equating the total moments with respect to the pivot point of the pendulum to zero, yields

$$\begin{aligned}&m_p\ell_p^2\ddot{\psi} + m_p\ell_p[\ddot{w}(t,L)\cos\,\alpha + \ddot{u}_1(t,L)\sin\,\alpha + \ddot{y}_g]\sin\,\psi \\ &+ m_p\ell_p[\ddot{u}_1(t,L)\cos\,\alpha - \ddot{w}(t,L)\,\sin\,\alpha]\cos\,\psi = -m_p g\ell_p\,\sin\,\psi - c_p(\dot{\psi} + \dot{\theta}(t,L)),\end{aligned} \tag{20}$$

where

$$u(s,t) = \int_0^s (\sqrt{1-w'^2} - 1)\,\mathrm{d}s + y_{\mathrm{gu}} \to u_1(s,t) = \int_0^s (\sqrt{1-w'^2} - 1)\,\mathrm{d}s \tag{21}$$

and c_p is the damping coefficient of the pendulum. Eq. (20) includes the terms $\dot{\theta}$ and $\ddot{u}_1$ which need to be defined in terms of w. For this purpose, Eq. (21) is expanded by using binominal expansion and, by eliminating terms of order higher than three, yields

$$\ddot{u}_1 = -\int_0^L (\dot{w}'^2 + w'\ddot{w}')\,\mathrm{d}s. \tag{22}$$

Differentiating (from inextensibility condition) $w' = \sin(\theta)$ once with respect to time, and expanding the resulting equation using a binominal expansion result in

$$\dot{\theta} = \dot{w}' + \tfrac{1}{2}\dot{w}'w'^2, \tag{23}$$

where $\dot{\theta}$ is the angular velocity of the beam. To obtain the final pendulum equation, substituting Eqs. (22) and (23) into Eq. (20) gives

$$\ddot{\psi} + \frac{1}{\ell_p}[\ddot{w}(t,L)\cos(\alpha) + \ddot{u}_1(t,L)\sin(\alpha) + \ddot{y}_g + g]\sin\psi + \frac{1}{\ell_p}[\ddot{u}_1(t,L)\cos(\alpha) - \ddot{w}(t,L)\sin(\alpha)]\cos\psi + \frac{c_p}{m_p\ell_p^2}\left\{\dot{\psi} + \left[\dot{w}' + \frac{1}{2}\dot{w}'w'^2\right]_{s=L)}\right\} = 0. \tag{24}$$

By using the Newton's second law, the joint forces on the pendulum pivot point shown in Fig. 2 can be easily obtained. The forces acting on the beam can be easily calculated because of the equilibrium of the forces at joint:

$$\sum F_{\text{external}} = \sum F_{\text{effective}} \text{ on the pendulum}, \quad \sum F = 0 \text{ at the joint of the pendulum}, \tag{25}$$

$$F_{\text{pu}} = -F_{\text{bu}} = m_p\ell_p[\ddot{\psi}\cos(\psi-\alpha) - \dot{\psi}^2\sin(\psi-\alpha)], \tag{26}$$

$$F_{\text{pv}} = -F_{\text{bv}} = m_p\ell_p[\ddot{\psi}\sin(\psi-\alpha) + \dot{\psi}^2\cos(\psi-\alpha)]. \tag{27}$$

2.2. Linear undamped problem

The governing Eq. (18) is nonlinear, and does not admit a closed-form solution. Therefore, an approximate solution will be sought that satisfies both the equation and the boundary conditions. We represent the solution of the nonlinear problem in the form

$$w(s,t) = \sum_n \phi_n(s)q_n(t), \tag{28}$$

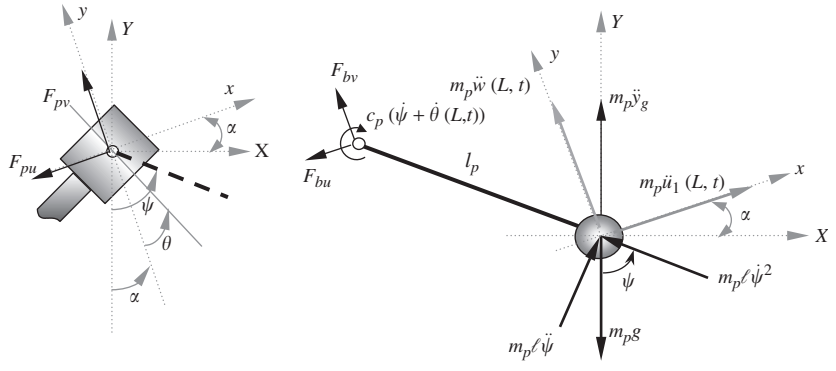

Fig. 2. Free body diagram of the pendulum.

where $\phi_n(s)$ is the shape function of the nth linear mode, and $q_n(t)$ is the time modulation of the nth mode. The undamped linear free vibration problem under axial loading is governed by

$$EIw'''' + \rho Ag\,\sin(\alpha)[(\ell - s)w']' + mg\,\sin(\alpha)w'' + \rho A\ddot{w} = 0, \tag{29}$$

which is subject to the boundary condition (7–8). The unimodal solution of this problem is obtained by applying Adomian decomposition method [14–16]:

$$\begin{aligned}\phi(s) = {} & 0.5s^2 - 0.10877\sin(\alpha)s^4 + 0.42336\times10^{-1}\sin(\alpha)s^5 + [0.94654\times10^{-2}\sin^2(\alpha)\\ & + 0.35963\times10^{-3}\omega^2]s^6 - 0.78944\times10^{-2}\sin^2(\alpha)s^7 + \cdots + C_2/C_1\{0.16\bar{6}s^3\\ & - 0.021754\sin(\alpha)s^5 + 0.10584\times10^{-1}\sin(\alpha)s^6 + [0.51376\times10^{-4}\omega^2 + 0.13522\\ & \times10^{-2}\sin^2(\alpha)]s^7 - 0.13157\times10^{-2}\sin^2(\alpha)s^8\ldots\},\end{aligned} \tag{30}$$

where

$$\begin{aligned}C_2/C_1 = {} & -[1 - 0.12359\sin(\alpha) + 0.26844\times10^{-2}\sin^2(\alpha) + 0.1619\times10^{-3}\omega^2 - 0.34517\\ & \times10^{-5}\sin(\alpha)\omega^2 - 0.45423\times10^{-4}\sin^3(\alpha)]/[0.35 - 0.13889\times10^{-1}\sin(\alpha)\\ & + 0.16283\times10^{-3}\sin^2(\alpha) + 0.11333\times10^{-4}\omega^2].\end{aligned} \tag{31}$$

2.3. Temporal problem

Eqs. (18) and (24) are coupled nonlinear equations which characterize the dynamics of the beam–pendulum system. The system of equations does not have closed-form solutions. The model is governed by a set of partial differential equations which involve infinite modal series. The Galerkin method is used to obtain a set of ordinary differential equations form of given partial differential equations for an approximate solution. In this study, it is assumed that the first mode of the system is dominant, therefore, for the first mode, the truncated displacement function becomes

$$w = \phi(s)q(t). \tag{32}$$

By substituting Eq. (32) into the partial differential Eqs. (18) and (24) and orthogonalizing the error with respect to the eigenfunction, the following ordinary differential equations are obtained for the beam and pendulum, respectively:

$$\begin{aligned}&[\Re_1 - \Re_2 q^2]\ddot{q} + \Re_4\dot{q} + \Re_3 q^3 - \Re_2 q\dot{q}^2 + \Re_7\ddot{y}_{gv} - K_8F_{pv}\\ &\quad + [\Re_5 + \Re_6[\ddot{y}_{gu} + g]\sin(\alpha) + K_7F_{pu}]q = 0,\end{aligned} \tag{33}$$

$$\begin{aligned}&\ddot{\psi} + \frac{1}{\ell_p}[\Re_8\ddot{q}\cos(\alpha) - \Re_9(\dot{q}^2 + q\ddot{q})\sin(\alpha) + \ddot{y}_g + g]\sin(\psi)\\ &\quad + \frac{1}{\ell_p}[-\Re_9(\dot{q}^2 + q\ddot{q})\cos(\alpha) - \Re_8\ddot{q}\,\sin(\alpha)]\cos(\psi) + \frac{c_p}{m_p\ell_p^2}\dot{\psi} + \frac{c_p}{m_p\ell_p^2}[\Re_{11}\dot{q} + \Re_{10}\dot{q}q^2] = 0,\end{aligned} \tag{34}$$

where $\Re_1\ldots\Re_{11}$ are the Galerkin coefficients of the beam and the pendulum, respectively and defined in Appendix. Eq. (33) including the first mode terms of the beam–pendulum system is ready for the numerical analysis. The equations of motion of the beam and the pendulum (33, 34) which were transformed into four first-order systems were solved by using Runge–Kutta method. This method is extremely accurate, however, it requires fewer steps for a desired level of accuracy than other methods. This makes it a favorite in numerical integration of nonlinear differential equation.

3. Results and discussions

Runge–Kutta method was used for the numerical integration. The results of the integration are presented for the following system parameters: $\rho A = 0.3925\,\text{kg/m}$, $m_T = 0.212\,\text{kg}$, $L = 0.35\,\text{m}$ $EI = 1.5158\,\text{N/m}^2$, $c = 0.07\,\text{kg s/m}$, $c_p = 0.025\,\text{kg/s}$. The system parameters are varied such that the range of the internal frequency ratio is $\omega_p/\omega_b = 0.46$–0.54, the mass ratio is $m_p/m_T = 0.01$–1.0, and the forcing amplitude is $y_g = 0.00025$ and $0.001\,\text{m}$. The natural frequency of the structure with the absorber locked comes out to be $\omega_b = 3.0\,\text{Hz}$.

To observe the dynamics of the system, three different analyses were performed numerically. The first indicates that the beam and the pendulum response is a function of forcing frequency at different orientation angles. The figures obtained from the first analysis include data obtained by sweeping the range between two forcing frequencies where the natural frequency of the beam lies. Hence, the border of the autoparametric region (absorption region) was observed from this sweep.

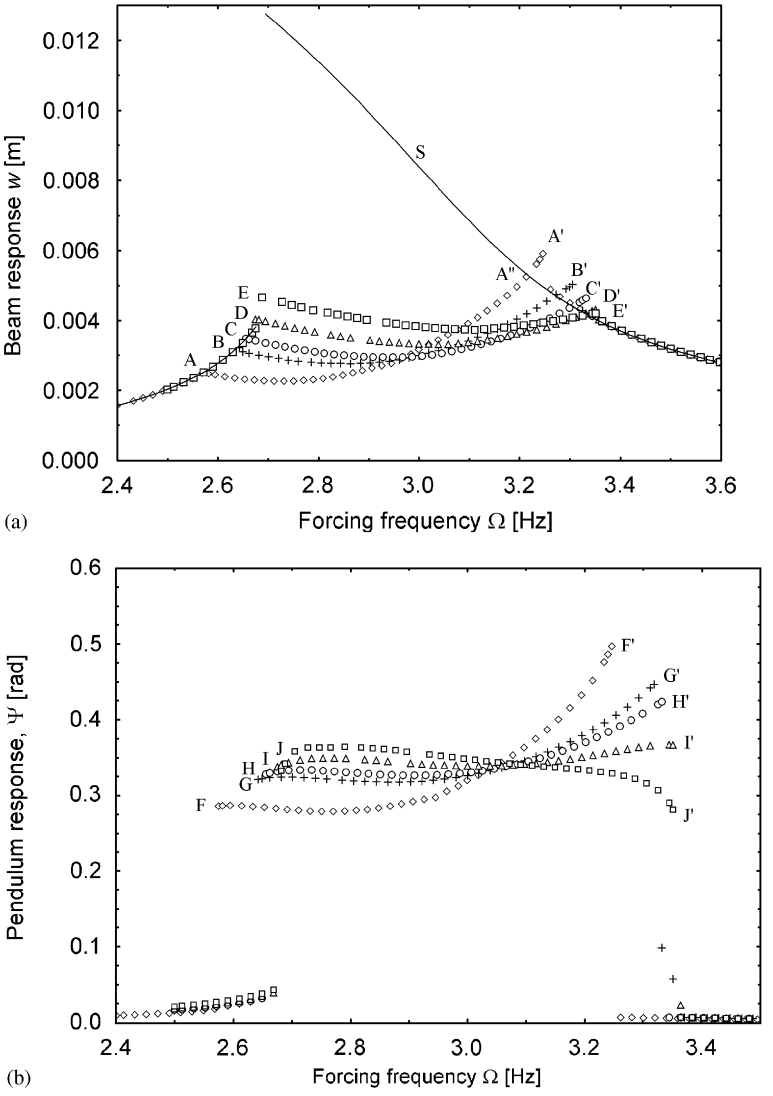

Fig. 3. Frequency response curves for $\alpha = 0°$: (a) beam response, (b) pendulum response. ($\diamond$) $\omega_p/\omega_b = 0.46$, ($+$) $\omega_p/\omega_b = 0.48$, ($\circ$) $\omega_p/\omega_b = 0.50$, ($\triangle$) $\omega_p/\omega_b = 0.52$, ($\square$) $\omega_p/\omega_b = 0.54$, and (—) beam response with locked pendulum.

The second analysis includes the effect of different mass ratios (m_p/m_T) and orientation angle on the absorption region. For this analysis, the internal frequency ratio ($\omega_p/\omega_b = 0.5$), the natural frequency ($\omega_b = 3.0$ Hz), and the forcing amplitude are taken to be constant during the numerical analysis. The figure of this analysis shows data points that refer to the jump frequencies of the beam during sweep.

The third analysis shows the effect of forcing amplitude and orientation angle on the absorption region. For this analysis, the mass ratio ($m_p/m_T = 0.125$), the internal frequency ratio ($\omega_p/\omega_b = 0.5$), and the natural frequency ($\omega_b = 3.0$ Hz) are taken to be constant. The figure obtained from this analysis show numerical data points that refer to the jump frequencies of the beam during sweep.

The frequency response curves of the cantilever beam (with and without the absorber) and the absorber for internal detuning ratios of 0.46, 0.48, 0.50, 0.52, and 0.54 respectively are shown in Fig. 3. The internal detuning ratio is defined as ω_p/ω_b. The curve S was obtained with the absorber locked for sweep while the other curves were obtained with the absorber activated for the sweep. The curve S indicates the characteristic response of the absorber locked for the sweep, while the curves (A, B, C, D, E) and (F, G, H, I, J) represents the characteristic response of the cantilever beam with the tip mass and the absorber for the sweep,

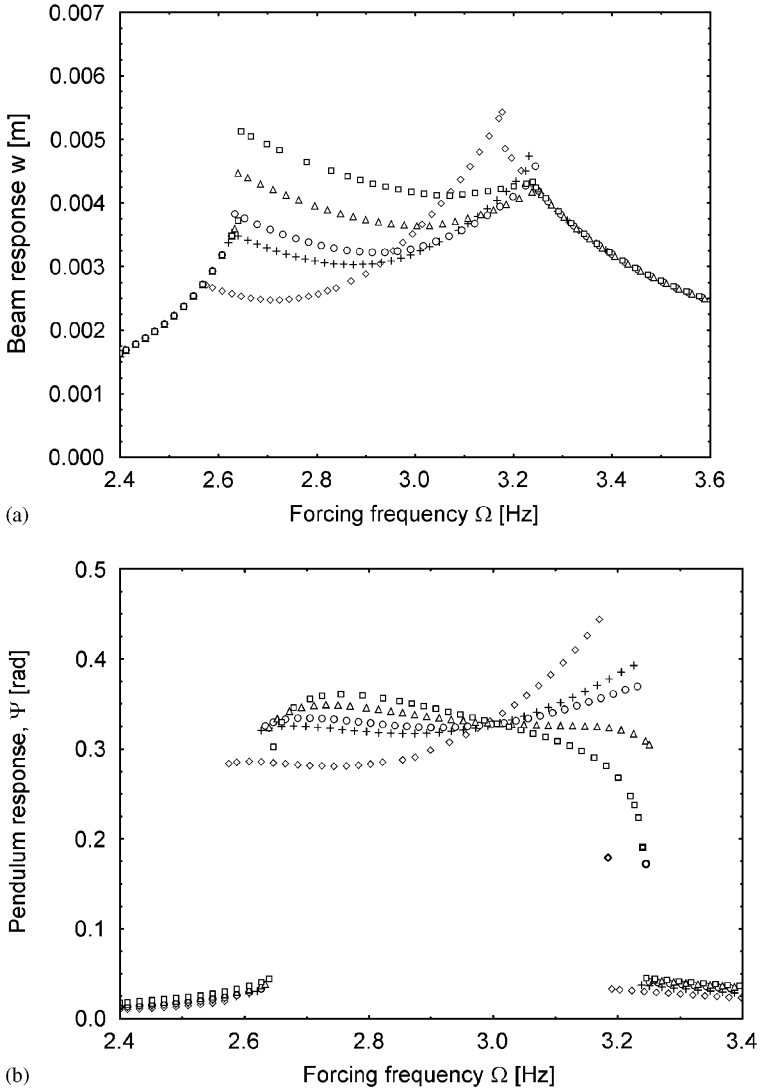

Fig. 4. Frequency response curves for $\alpha = 20^\circ$: (a) beam response, (b) pendulum response, ($\diamond$) $\omega_p/\omega_b = 0.46$, ($+$) $\omega_p/\omega_b = 0.48$, ($\circ$) $\omega_p/\omega_b = 0.50$, ($\triangle$) $\omega_p/\omega_b = 0.52$, and ($\square$) $\omega_p/\omega_b = 0.54$.

respectively. Curves A–E in Fig. 3a correspond to curves F–J in Fig. 3b, respectively. The cantilever beam response, curves A–E, and the absorber response, curves F–J, are given to show the unidirectional energy transfer between the modes.

In Fig. 3, the mass ratio ($m_p/m_T = 0.254$), and forcing amplitude ($y_g = 0.0005$ m) were selected as constant to obtain the curves (A–E) with and without the vibration absorber. These curves clearly show that the absorber effectively reduces the peak amplitude of the cantilever beam (primary structure). On these curves, the jump phenomenon was observed such as A for the cantilever beam and F for the pendulum during the sweep. From this figure, it is clear that point A for the cantilever beam and point F for the absorber show the starting points of the interaction between the modes during the sweep. The region between starting points, A and A' or F and F', is called the absorption region. This type of energy interaction has been reported by other researchers while investigating nonlinear coupled oscillators [4,10,11]. From Fig. 3a, it is also clear that within the absorption region the amplitude of the primary structure is lower when the absorber is used. In this region,

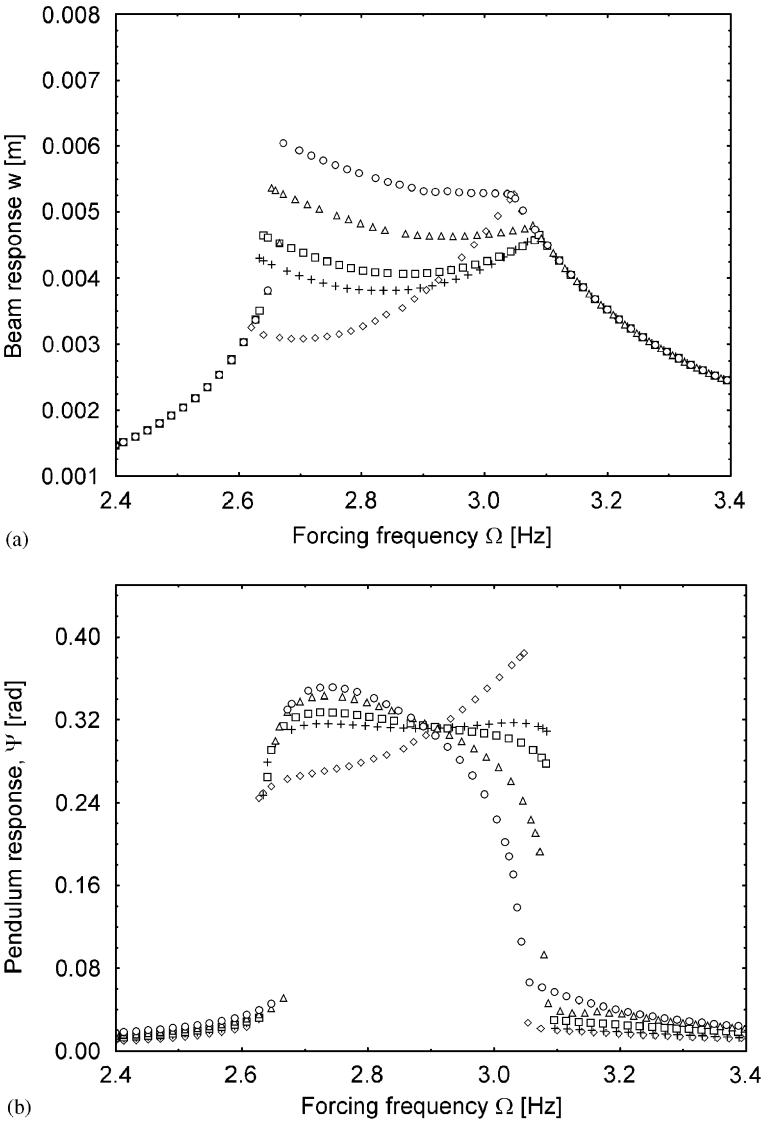

Fig. 5. Frequency response curves for $\alpha = 40^\circ$: (a) Beam response, (b) pendulum response, ($\diamond$) $\omega_p/\omega_b = 0.46$, ($+$) $\omega_p/\omega_b = 0.48$, ($\square$) $\omega_p/\omega_b = 0.50$, ($\triangle$) $\omega_p/\omega_b = 0.52$, and ($\circ$) $\omega_p/\omega_b = 0.54$.

the minimum response of the primary structure is observed at the point which satisfied the autoparametric conditions ($\Omega = \omega_b = 2\omega_p$). It is important to note that when the curve AA' is investigated, the energy transfer occurs from the absorber to the primary structure at the points between A'' and A'. Therefore, the region between points A'' and A' is called the non-absorption region. When the figure is examined, the variation of the internal detuning ratio changes the absorption region. As can be seen from this variation, the internal detuning ratio should be 0.5 for the maximum energy interaction between the modes. It is clear that if the internal detuning ratio is lower or higher than 0.5, unidirectional energy transfer between the modes gets worse in the absorption region.

Figs. 4–6 show frequency response curves of the cantilever beam with the absorber and the absorber for the orientation angle of 20°, 40°, and 60°, respectively. As seen from the figures, the absorption region becomes narrow as the orientation angle varies; hence the jump points also change. While the maximum energy transfer between the beam and pendulum occurs at $\omega_p/\omega_b = 0.5$ as $\alpha = 0$ that indicates horizontal position of the

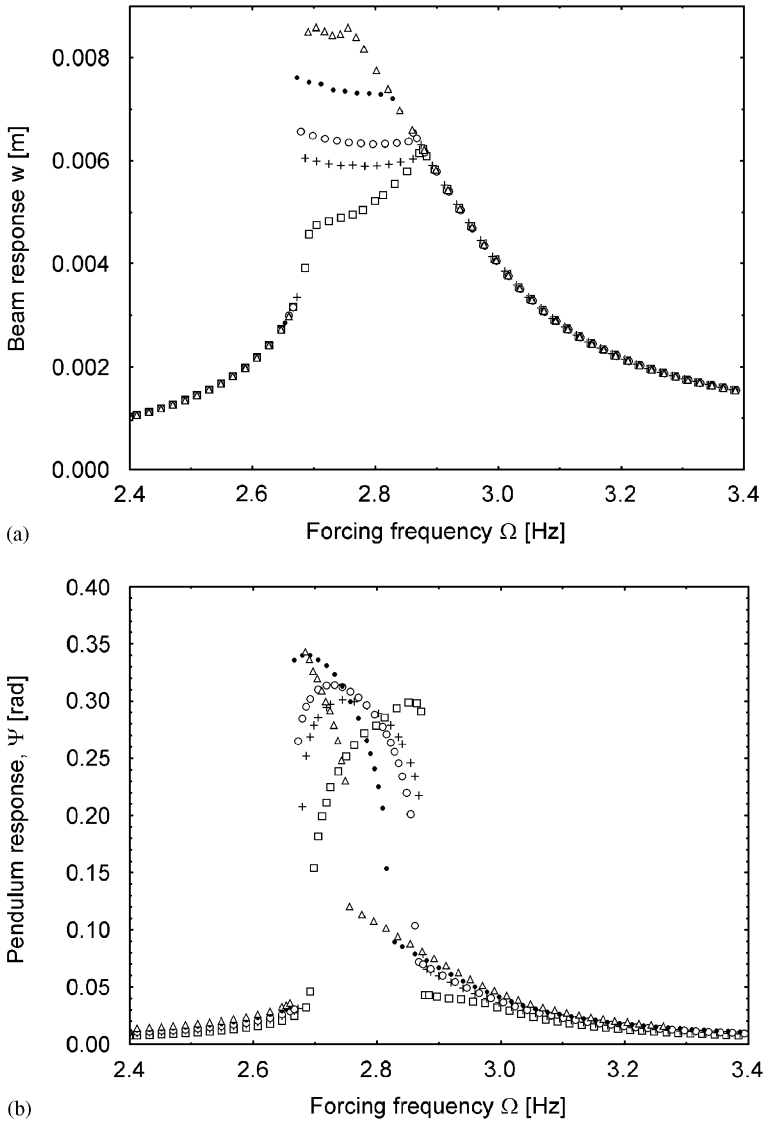

Fig. 6. Frequency response curves for $\alpha = 60°$: (a) beam response, (b) pendulum response, (□) $\omega_p/\omega_b = 0.46$, (+) $\omega_p/\omega_b = 0.48$, (○) $\omega_p/\omega_b = 0.50$, (●) $\omega_p/\omega_b = 0.52$, and (△) $\omega_p/\omega_b = 0.54$.

beam, this situation totally changes for $\alpha = 20^\circ$, 40°, and 60°. For instance, while the maximum energy transfer occurs at $\omega_p/\omega_b = 0.48$ as the beam is directed at the angle of 40° from the horizontal; i.e. $\alpha = 40^\circ$, the maximum energy transfer for $\alpha = 60^\circ$ occurs at $\omega_p/\omega_b = 0.46$. This could be explained as follows: when the orientation angle of the beam increases, the natural frequency of the beam decreases since the axial force gets larger. Because the autoparametric condition was set up for the horizontal position of the beam, this situation violates the autoparametric condition between the beam and pendulum. However, it can be seen that the maximum energy transfer occurs at around the value of $\omega_p/\omega_b = 0.48$ and $\omega_p/\omega_b = 0.46$ as the orientation angle of the beam becomes 40° and 60° since the new autoparametric conditions occur at these values due to the variation in the value of ω_p/ω_b.

Fig. 7 shows the variations of the absorption region with respect to the mass ratio for orientation angle of 0°, 20°, 40°, and 60°. To obtain these curves in the figure, the internal detuning ratio (0.5), and the forcing amplitudes (0.0005 m) were taken to be constant, and the mass ratio is varied from 0.1 to 1.0. For different mass ratios, the curves presented in Fig. 7 are obtained from the frequency response curves; i.e. from the figure between 3 and 6. In these figures, points A and A'' are used to construct the curves in the figure which show the variations of the jump points with respect to mass ratio during sweep. It is also observed that the mass ratio has no significant effect on the absorption region at a constant forcing amplitude if the absorber mass is greater than 30% of the main mass. In other words, a mass ratio of 0.3 provides large ranges of the absorption region. However, if the mass ratio is between 0.2 and 0.3, there is some of noticeable change in the absorption region. In addition, if the mass ratio is less than 0.2, the absorption region becomes very narrow. Therefore, if the absorber mass is between 20% and 30% of the main mass, a sufficiently wide absorption region in the neighborhood of the autoparameteric region is obtained. The absorption region dramatically becomes narrow as the orientation angle increases. In the case that the beam was inclined to 60°, there is no absorption region observed for the mass ratio less than 20%, which indicates that the system is out of the autoparametric condition.

Fig. 8 shows the variations of the absorption region with the forcing amplitude. To obtain this figure, the mass ratio (0.254) and the internal frequency ratio (0.5) were selected to be as constant, and the forcing amplitude was varied from 0.0001 to 0.0015 m for the analysis. The figure was obtained from the frequency response curves for the orientation angles of 0°, 20°, 40°, and 60°. The curves show the variation of the jump points with the forcing amplitude during the sweep. It is observed that the regions in Fig. 8 vary with the forcing amplitude and orientation angle. Higher forcing amplitudes provide larger absorption regions, whereas higher orientation angle narrow absorption regions.

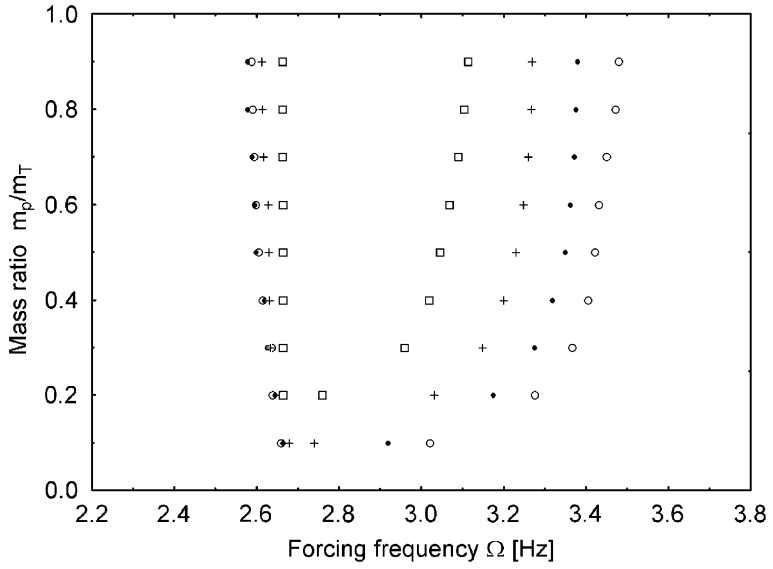

Fig. 7. Variation of absorption region with respect to mass ratio: (○) $\alpha = 0^\circ$, (●) $\alpha = 20^\circ$, (+) $\alpha = 40^\circ$, and (□) $\alpha = 60^\circ$.

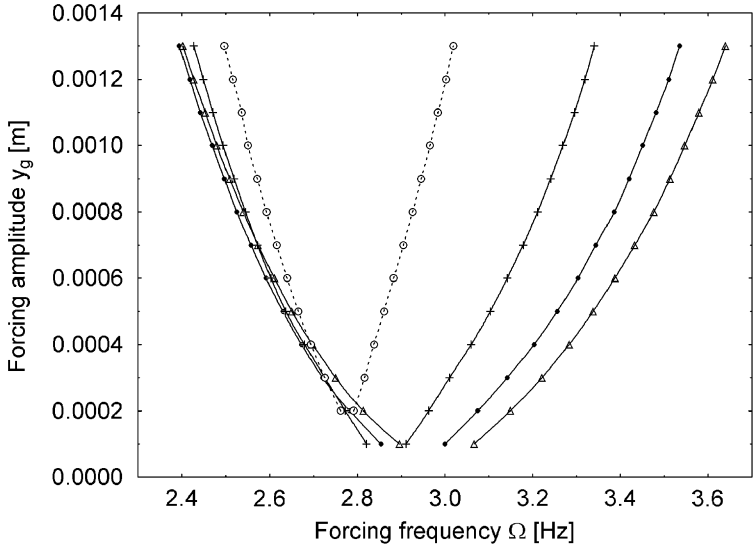

Fig. 8. Variation of absorption region with respect to forcing amplitude: (–△–) $\alpha = 0^\circ$, (–●–) $\alpha = 20^\circ$, (–+–) $\alpha = 40^\circ$, and (–○–) $\alpha = 60^\circ$.

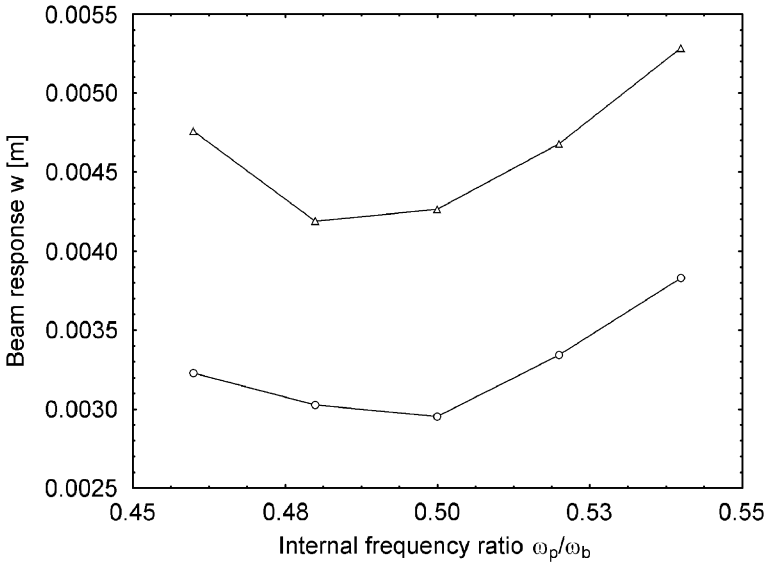

Fig. 9. The response of the beam at the resonance frequency with respect to internal frequency ratio: (○) $\alpha = 0^\circ$ and (△) $\alpha = 60^\circ$.

Fig. 9 shows the response of the beam at the resonance frequency with respect to internal frequency ratio. The values of the response of the beam at the resonance frequency from the frequency response curves (for instance, Figs 3 and 6) are constructed to obtain the curves in Fig. 9. This figure clearly shows that the maximum energy transfer occurs at the internal frequency ratio of 0.5 for the orientation angle of 0° and around the internal frequency ratio of 0.48 for the orientation angle of 60° because of the variation of natural frequency of the beam. At these points, response of the beam is a minimum. When the internal frequency ratio deviates from 0.5 or from 0.48, response of the beam increases. When the internal frequency ratio is far greater or less than 0.5 or 0.48, the coupling between the beam and pendulum cannot be observed. At those internal frequency ratios, the energy transfer does not occur.

4. Conclusions

The basic absorption action of the autoparametric system under sinusoidal excitation was comprehensively investigated numerically. This study involves defining an absorption region for the absorber depending on the control parameters, which are the internal detuning ratio, mass ratio, forcing amplitude, and orientation angle. As a result, the effects of these parameters on the absorption region were established by conducting sweep. The numerical results indicate that the beneficial unidirectional energy transfer occurs between the cantilever beam with the tip mass and the absorber when the autoparametric condition, $\Omega = \omega_b = 2\omega_p$, is satisfied. However, the effect of the absorber on the absorption region is related to the internal detuning ratio and orientation angle. When the detuning ratio and the orientation angle deviates the unidirectional energy transfer between the modes become less. Therefore, the beneficial effect of the absorber depends on the internal detuning ratio and orientation angle. In addition, this study shows that while the higher forcing amplitudes result in larger absorption regions, the increase of the orientation angle narrows these regions. It is also observed that beneficial effect of the absorber resulting from increasing mass ratio disappear when the mass ratio is lower than 0.1 or higher than 0.3.

Appendix

$$K_1 = \int_0^L \phi^2 \,\mathrm{d}s,$$

$$K_2 = \int_0^L \phi'''' \phi \,\mathrm{d}s,$$

$$K_3 = \int_0^L \phi[\phi'(\phi'\phi'')']' \mathrm{d}s,$$

$$K_4 = \int_0^L \phi \left[\phi' \int_s^L \int_0^s \phi'^2 \,\mathrm{d}s \,\mathrm{d}s\right]' \mathrm{d}s,$$

$$K_5 = \int_0^L \phi \left[\phi' \int_0^L \phi'^2 \,\mathrm{d}s\right]' \mathrm{d}s,$$

$$K_6 = \int_0^L \phi[\phi'\{L-s\}]' \,\mathrm{d}s,$$

$$K_7 = \int_0^L \phi[\phi']' \mathrm{d}s,$$

$$K_8 = \int_0^L \phi\delta(s-(L-\varepsilon)) \,\mathrm{d}s,$$

$$K_9 = \int_0^L \phi \,\mathrm{d}s,$$

$$\Re_1 = \rho A K_1, \Re_2 = \rho A K_4 + m K_5, \Re_3 = EI K_3, \Re_4 = c K_1, \Re_5 = EI K_2,$$
$$\Re_6 = \rho A K_6 + m K_7, \Re_7 = \rho A K_9 + m K_8, \Re_8 = \phi_{(L)}, \Re_9 = \int_0^L \phi'^2 \,\mathrm{d}s, \Re_{10} = \tfrac{1}{2}\phi'^3_{(L)}, \Re_{11} = \phi'_{(L)}.$$

References

[1] L.D. Zavodney, A.H. Nayfeh, The non-linear response of a slender beam carrying lumped mass to principal parametric resonance: theory and experiment, *International Journal of Nonlinear Mechanics* 24 (1989) 105–125.
[2] M.R.M. Crespo da Silva, C.L. Zaretzky, D.H. Hodges, Effects of approximations on the static and dynamic response of a cantilever with a tip mass, *International Journal of Solids and Structures* 27 (5) (1991) 565–583.
[3] R.S. Haxton, A.D.S. Barr, The autoparametric vibration absorber, Transactions of the American Society of Mechanical Engineers, *Journal of Engineering for Industry* 94 (1972) 119–125.
[4] A. Ertas, O. Cuvalci, S. Ekwaro-Osire, Performance of pendulum absorber for a nonlinear system of varying orientation, *Journal of Sound and Vibration* 229 (4) (2000) 913–933.
[5] J.Q. Sun, M.R. Jolly, M.A. Morris, Passive, adaptive and active tuned vibration absorbers—a survey, *Journal of Mechanical Design* 117 (1995) 234–242.
[6] R.G. Jacquot, Optimal vibration absorbers for general beam system, *Journal of Sound and Vibration* 60 (1978) 535–542.
[7] L. Kitis, B.P. Wang, W.D. Pilkey, Vibration reduction over a frequency range, *Journal of Sound and Vibration* 89 (4) (1983) 559–569.
[8] I.N. Jordanov, B.I. Cheshankov, Optimal design of linear and non-linear dynamic vibration absorbers, *Journal of Sound and Vibration* 123 (1988) 157–170.
[9] T. Dahlberg, On optimal use of the mass of a dynamic vibration absorber, *Journal of Sound and Vibration* 132 (1989) 518–522.
[10] O. Cuvalci, The effect of detuning parameters on the absorption region for a coupled system: a numerical and experimental study, *Journal of Sound and Vibration* 229 (4) (2000) 837–857.
[11] M. Yaman, S. Sen, The analysis of the orientation effect of non-linear flexible systems on performance of the pendulum absorber, *International Journal of Non-Linear Mechanics* 39 (5) (2004) 741–752.
[12] S.R. Bishop, D.L. Xu, M.J. Clifford, Flexible control of the parametrically excited pendulum, *Proceedings of the Royal Society of London*, A 452, 1996, pp. 1789–1806.
[13] S.S. Oueini, A.H. Nayfeh, J.R. Pratt, A nonlinear vibration absorber for flexible structures, *Nonlinear Dynamics* 15 (1998) 259–282.
[14] G. Adomian, A review of the decomposition method in applied mathematics, *Journal of Mathematical Analysis and Applications* 135 (2) (1988) 501–544.
[15] G. Adomian, Solving frontier problems modelled by nonlinear partial differential equations, *Computers & Mathematics with Applications* 22 (8) (1991) 91–94.
[16] A.M. Wazwaz, Analytic treatment for variable coefficient fourth-order parabolic partial differential equations, *Applied Mathematics and Computation* 123 (2001) 219–227.
[17] L. Meirovitch, *Analytical Methods in Vibrations*, The Macmillan Company, London, 1967.